Tunable Streaming Current in a pH-Regulated Nanochannel by a Field Effect Transistor

ARTICLE *in* THE JOURNAL OF PHYSICAL CHEMISTRY C · MARCH 2014

Impact Factor: 4.77 · DOI: 10.1021/jp500996b

4 AUTHORS, INCLUDING:

Li-Hsien Yeh
National Yunlin University of Science and Tec…

Yu Ma
Harbin Institute of Technology

Shizhi Qian
Old Dominion University

THE JOURNAL OF PHYSICAL CHEMISTRY C

Article

pubs.acs.org/JPCC

Tunable Streaming Current in a pH-Regulated Nanochannel by a Field Effect Transistor

Song Xue,[†,‡] Li-Hsien Yeh,*[,†,§] Yu Ma,[∥] and Shizhi Qian*[,‡]

[‡]Institute of Micro/Nano Technology, Old Dominion University, Norfolk, Virginia 23529, United States

[§]Department of Chemical and Materials Engineering, National Yunlin University of Science and Technology, Yunlin 64002, Taiwan

[∥]School of Energy Science and Engineering, Harbin Institute of Technology, Harbin 150001, People's Republic of China

Supporting Information

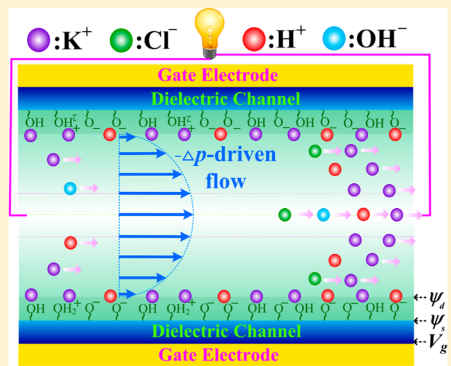

ABSTRACT: Many experimental results demonstrated that ion transport phenomena in nanofluidic devices are strongly dependent on the surface charge property of the nanochannel. In this study, active control of the surface charge property and the streaming current, generated by a pressure-driven flow, in a pH-regulated nanochannel using a field effect transistor (FET) are analyzed for the first time. Analytical expressions for the surface charge property and the streaming current/conductance have been derived taking into account multiple ionic species, surface chemistry reactions, and the Stern layer effect. The model is validated by the experimental data of the streaming conductance in the silica nanochannel available in the literature. Results show that the pH-dependent streaming conductance of the gated silica nanochannel is consistent with its modulated zeta potential; however, the salt concentration-dependent streaming conductance might be different from the zeta potential behavior, depending on the solution pH and the gate potential imposed. The performance of the field effect modulation of the zeta potential and the streaming conductance is significant for lower solution pH and salt concentration. The results gathered are informative for the design of the next-generation nanofluidics-based power generation apparatus.

1. INTRODUCTION

Recent advances in nanofluidics attract considerable attention in using them as promising platforms for diverse applications such as ionic gates,[1,2] ionic diodes,[3−5] energy conversion,[6−10] and single (bio)nanoparticle sensing.[11−13] All of these nanofluidic-based applications rely on accurately analyzing the resulting ionic current signals, determined by the ion transport phenomena in these nanofluidic devices, in various solution properties.[14−16] Many experimental results revealed that the ion transport in nanofluidics can be regulated by modulating the surface charge property at the solid/liquid interface of these nanofluidic devices.[17−19] Therefore, active control of the surface charge property of nanofluidic devices in various solution properties is crucial for the development of next-generation nanofluidics-based apparatus.

To this end, nanofluidic field effect transistors (FETs),[20−26] consisting of electrically controllable gate electrodes patterned along the outer wall surface of the dielectric nanochannels (or nanopores) made of such as silicon dioxide (SiO_2), silicon nitride (SiN_x), and aluminum oxide (Al_2O_3), have been developed to actively modulate their surface charge property. Control of the surface charge property, in turn, controls the transport of ions, fluid, and biomolecules in nanofluidics by modulating the gate potential imposed on the gate electrode. Many theoretical efforts[27−40] have been made to reveal how to regulate the transport of ions, fluid, and biomolecules in the FET-gated nanofluidic devices. However, these studies have several limited assumptions, such as a constant surface charge density at the dielectric nanochannel wall,[28−36] consideration of background ionic species only,[27−40] and without considering the Stern layer effect.[28−39] Recently, Guan et al.[41] experimentally demonstrated that the field effect modulation of zeta potential and surface charge density at the gated dielectric channel material (e.g., SiO_2 and SiN_x)/electrolyte interface in various solution pH and ionic strength is distinctly different. They concluded that these intrinsic differences result from the surface chemistry reactions of functional groups with H^+ ions at the dielectric/electrolyte interface. Thus, developing a more general and realistic model to elaborate experimental observations in relevant gated nanofluidic devices is highly desirable.

Recent experimental studies demonstrated that the streaming current, generated by the pressure-driven flow, in the nanochannel provides a simple and effective scenario for converting hydrodynamics to electrical power.[6−10] This clean energy harvesting system using nanofluidics might open a new way for the development of renewable energy resources.[9] The experimental results show that the streaming current is dependent on the flow of excess counterions, driven by an applied pressure field, in the electric double layer (EDL)

Received: January 28, 2014
Revised: March 3, 2014
Published: March 4, 2014

formed in the vicinity of the charged channel wall.[42] This implies that the surface charge property of the nanochannel and net amount of mobile ionic species in various electrolyte solutions can significantly influence the streaming current behavior. Although several theoretical works have been made for the streaming current in the nanochannel, all of these studies assumed that the liquid phase only contains one kind of cation and anion from the background salt.[6−8,42−48] This assumption, although it simplifies the mathematical analysis, is unrealistic in practice because other ionic species are usually present. For example, the presence of H^+ and OH^- ions need to be considered inevitably when the solution pH appreciably deviates from neutral.

In an attempt to better understand the aforementioned influences on the streaming current in the nanochannel, we investigate the field effect modulation of the surface charge property and the streaming current/conductance in a long pH-regulated nanochannel under various solution properties (pH and background salt concentration). Analytical expressions are derived for the first time to predict the zeta potential and the streaming current/conductance with the consideration of FET, multiple ionic species, surface chemistry reactions on the dielectric channel wall, and the Stern layer effect. In contrast to most of existing studies on the ion transport in nanofluidics, which focused mainly on the numerical simulations,[8,27−35,37,38,43−46] the present analytical results would provide better insight into the underlying physics and present convenient recipes for utilizing gated nanochannels in relevant applications.

2. THEORETICAL ANALYSIS

As schematically shown in Figure 1, we consider a fully developed pressure-driven flow of an aqueous electrolyte solution of relative permittivity ε_f in a long pH-regulated nanochannel of height h, width w, and length l. A streaming

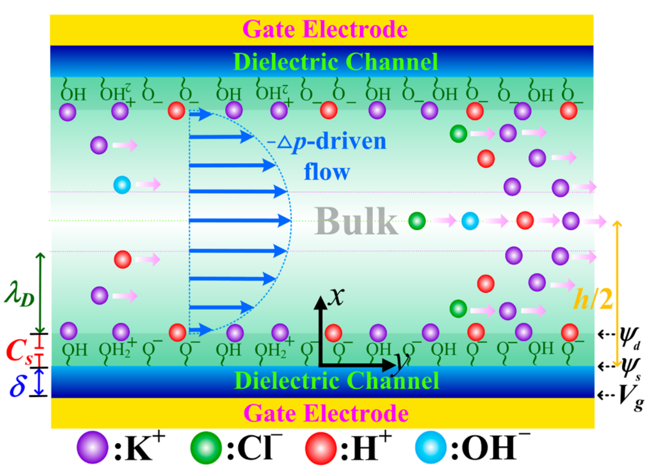

Figure 1. Schematic representation of the field effect regulation of the zeta potential (ψ_d) and the streaming current, driven by an applied pressure field ($-\Delta p$), in a pH-regulated nanochannel containing multiple ionic species, H^+, K^+, Cl^-, and OH^-. Four major regions are considered: the dielectric channel of thickness δ, the immobile Stern layer with surface capacitance C_s, the diffusive layer of Debye length λ_D, and the bulk solution state of pH and background salt concentration C_{KCl}. V_g is the gate potential imposed on the gate electrode, and ψ_s is the surface potential stemming from the association and dissociation surface reactions of functional groups on the nanochannel wall.

current, I_{str}, is induced by a pressure gradient, $-\Delta p$, applied across the nanochannel.[42] The nanochannel is equipped with a FET, including a thin dielectric channel layer of thickness δ and relativity permittivity ε_d, and a gate electrode patterned on its outer surface. A gate potential, V_g, is imposed on the gate electrode to regulate the surface charge property and the streaming current in the nanochannel. The Cartesian coordinates x and y with the origin located at the bottom solid/liquid interface are adopted, and $-\Delta p$ is directed along the y-direction.

We assume the following: (i) The liquid phase is an incompressible Newtonian fluid containing N kinds of ionic species, and the pressure-driven flow is fully developed and parallel to the nanochannel wall (i.e., y-direction). (ii) The Stern layer of a very thin thickness δ_s is formed on the nanochannel wall, and ions and fluid inside that layer are immobile and do not contribute to streaming current. (iii) The no-slip plane is located at the Stern layer/diffusive layer interface. (iv) The dielectric channel (e.g., SiO_2, SiN_x, and Al_2O_3) wall in contact with an aqueous solution is of charge-regulated nature[45,49,50] and bears a uniform surface charge density σ_s along the y-direction. For example, nanochannels made of SiO_2 (or SiN_x) and Al_2O_3 bear, respectively, dissociable functional groups Si−OH[45,49] and Al−$OH^{-1/2}$,[27,50] capable of undergoing dissociation/association reactions with protons in aqueous solution. (v) The electroviscous effect is neglected, following the treatments of van der Heyden[6,7,42] and Chang and Yang.[47] (vi) The nanochannel height is much smaller than both its width and length ($h \ll w$ and $h \ll l$) so that the present problem can be approximated as a nanoslit with two infinite parallel plates. (vii) The overlapping of the EDLs of two adjacent nanochannel walls is insignificant, implying that the Debye length is much smaller than the half height of the nanochannel (i.e., $\lambda_D = \kappa^{-1} \ll h/2$). This assumption holds for most experimental conditions in nanofluidics. For example, the Debye length ranges from 9.6 to 0.3 nm, which is very thin compared to most of h,[7,51−53] for the background salt concentration in experiments varying from 1 to 1000 mM. Therefore, the possible presence of the ion concentration polarization,[14,54] arising from the selective transport of counterions and co-ions, can be neglected. Under above assumptions, the distributions of the electric potential, ionic concentrations, and the fluid velocity are uniform in the y-direction.

2.1. Governing Equations and Boundary Conditions.

Based on the aforementioned assumptions, the electric potentials within the dielectric channel, Stern layer, and liquid, ϕ, φ, and ψ, respectively, and the flow field can be described by

$$\frac{d^2\phi}{dx^2} = 0 \quad \text{within the dielectric channel} \quad (-\delta \le x \le 0) \tag{1}$$

$$\frac{d^2\varphi}{dx^2} = 0 \quad \text{within the Stern layer} \quad (0 \le x \le \delta_s) \tag{2}$$

$$\frac{d^2\psi}{dx^2} = -\frac{\rho_e}{\varepsilon_0\varepsilon_f} = -\frac{1}{\varepsilon_0\varepsilon_f}\sum_{i=1}^{N} Fz_iC_{i0}\exp\left(-\frac{z_iF\psi}{RT}\right)$$
$$\text{within the liquid phase} \quad (\delta_s \le x \le h/2) \tag{3}$$

dx.doi.org/10.1021/jp500996b | J. Phys. Chem. C 2014, 118, 6090−6099

$$\frac{d^2u_y}{dx^2} = \frac{1}{\mu}\frac{dp}{dy} \quad \text{within the liquid phase} \quad (\delta_s \le x \le h/2) \tag{4}$$

In the above, ρ_e is the mobile space charge density; z_i and C_{i0} are the valence and the bulk concentration of the ith ionic species, respectively; ε_0, F, R, and T are the absolute permittivity of vacuum, Faraday constant, universal gas constant, and absolute temperature, respectively; μ and u_y are the dynamic fluid viscosity and the fully developed pressure-driven fluid velocity in the y-direction, respectively.

The boundary conditions associated with eqs 1−4 are at the gate electrode ($x = -\delta$),

$$\phi = V_g \tag{5}$$

at the dielectric channel/Stern layer interface ($x = 0$),

$$\phi = \varphi = \psi_s \tag{6a}$$

$$-\varepsilon_0\varepsilon_d\frac{d\phi}{dx} + \varepsilon_0\varepsilon_f\frac{d\varphi}{dx} = -\sigma_s \tag{6b}$$

at the Stern layer/diffusive layer interface ($x = \delta_s$),

$$\varphi = \psi = \psi_d \tag{7a}$$

$$-\varepsilon_0\varepsilon_f\frac{d\varphi}{dx} + \varepsilon_0\varepsilon_f\frac{d\psi}{dx} = 0 \tag{7b}$$

$$u_y = 0 \tag{7c}$$

and at the center of the nanochannel ($x = h/2$),

$$\psi = \frac{d\psi}{dx} = 0 \tag{8a}$$

$$\frac{du_y}{dx} = 0 \tag{8b}$$

Equations 6a and 6b imply that the electric potential is continuous but the electric field, which satisfies the Gauss's law, is not at the dielectric channel/Stern layer interface due to the discontinuity of the dielectric permittivities (ε_d and ε_f). Equation 8a depicts that at the center of the nanochannel, the electric potential stemming from the charged nanochannel wall vanishes, and the ionic concentrations reach their bulk values due to the neglect of the EDL overlapping inside the nanochannel.

The analytical solutions to eqs 1 and 2 subject to eqs 5, 6a, and 7a are

$$\phi = \psi_s + \frac{\psi_s - V_g}{\delta}x \tag{9}$$

$$\varphi = \psi_s + \frac{\psi_d - \psi_s}{\delta_s}x \tag{10}$$

By substituting eqs 9 and 10 into eqs 6b and 7b and letting the surface capacitance of the Stern layer, $C_s = \varepsilon_0\varepsilon_f/\delta_s$, we obtain

$$-\varepsilon_0\varepsilon_d\left(\frac{\psi_s - V_g}{\delta}\right) + C_s(\psi_d - \psi_s) = -\sigma_s \tag{11}$$

$$-C_s(\psi_d - \psi_s) - \sigma_d = 0 \tag{12}$$

Here, σ_d is the surface charge density of the diffuse layer and can be expressed as

$$\begin{aligned}\sigma_d &= -\varepsilon_0\varepsilon_f d\psi/dx|_{x=\delta_s}\\ &= \text{sign}(\psi_d)\sqrt{2\varepsilon_0\varepsilon_f RT\sum_{i=1}^{N} C_{i0}\left[\exp\left(-\frac{z_iF\psi_d}{RT}\right) - 1\right]}\end{aligned} \tag{13}$$

where $\text{sign}(\psi_d) = 1$ for $\psi_d > 0$ and $\text{sign}(\psi_d) = -1$ for $\psi_d < 0$. It is worth noting that in the absence of the FET, the first term of the left-hand side of eq 11 vanishes and, therefore, eqs 11 and 12 reduce to

$$\psi_s - \psi_d = \frac{\sigma_s}{C_s} = \frac{\sigma_d}{C_s} \tag{14}$$

which is the well-known basic Stern layer model.[49] In short, the Stern layer models to describe the relationship between the surface potential (ψ_s) and zeta potential (ψ_d) of the nanochannel in the absence (eq 14) and presence (eqs 11 and 12) of FET are remarkably different.

Suppose that the dielectric channel wall bears dissociable functional groups MOH, capable of undergoing the following dissociation/association reactions: $MOH \leftrightarrow MO^- + H^+$ and $MOH + H^+ \leftrightarrow MOH_2{}^+$ with equilibrium constants $K_A = (\Gamma_{MO^-}[H^+]_s)/\Gamma_{MOH}$ and $K_B = \Gamma_{MOH_2{}^+}/(\Gamma_{MOH}[H^+]_s)$, respectively. Here, Γ_{MOH}, Γ_{MO^-}, and $\Gamma_{MOH_2{}^+}$ denote the surface site densities of MOH, MO^-, and MOH^{2+}, respectively; $[H^+]_s$ is the molar concentration of H^+ ions at the dielectric channel/liquid interface. If we let the total number site density of MOH molecules on the dielectric channel surface $N_{total} = \Gamma_{MOH} + \Gamma_{MO^-} + \Gamma_{MOH_2{}^+}$ and assume that the equilibrium distribution of H^+ ions follows the Boltzmann distribution, the surface charge density of the dielectric channel σ_s can be expressed as[40]

$$\begin{aligned}\sigma_s = -FN_{total}\Bigg\{\Bigg[10^{-pK_A} - 10^{-pK_B}\left[10^{-pH}\exp\left(-\frac{F\psi_s}{RT}\right)\right]^2\Bigg]\\ \Bigg/\Bigg[10^{-pK_A} + 10^{-pH}\exp\left(-\frac{F\psi_s}{RT}\right)\\ + 10^{-pK_B}\left[10^{-pH}\exp\left(-\frac{F\psi_s}{RT}\right)\right]^2\Bigg]\Bigg\}\end{aligned} \tag{15}$$

where $pK_j = -\log K_j$ (j = A and B).

To simulate experimental conditions, we assume that the background salt in aqueous electrolyte solution is KCl of background concentration C_{KCl}, and the solution pH is adjusted by HCl and KOH. This implies that four major kinds of ionic species (i.e., $N = 4$) including K^+, Cl^-, H^+, and OH^- need to be considered. Let C_{10}, C_{20}, C_{30}, and C_{40} (in mM) be their bulk concentrations, respectively. Electroneutrality yields the following relations:[55,56] $C_{10} = C_{KCl}$, $C_{20} = C_{KCl} + 10^{(-pH+3)} - 10^{-(14-pH)+3}$, $C_{30} = 10^{(-pH+3)}$, and $C_{40} = 10^{-(14-pH)+3}$ for pH ≤ 7; $C_{10} = C_{KCl} - 10^{(-pH+3)} + 10^{-(14-pH)+3}$, $C_{20} = C_{KCl}$, $C_{30} = 10^{(-pH+3)}$, and $C_{40} = 10^{-(14-pH)+3}$ for pH > 7.

2.2. Analytical Multi-Ion Model (MIM). The electroneutrality condition results in $C_0 = C_{10} + C_{30} = C_{20} + C_{40} = C_{KCl} + 10^{(-pH+3)}$ for pH ≤ 7 and $C_{KCl} + 10^{-(14-pH)+3}$ for pH > 7. Equation 3, therefore, can be rewritten as

$$\frac{d^2\psi}{dx^2} = \frac{RT\kappa^2}{zF}\sinh\left(\frac{zF\psi}{RT}\right) \quad \text{within the liquid phase} \quad (\delta_s \le x \le h/2) \tag{16}$$

where $z = z_1 = -z_2$ and $\kappa^{-1} = \lambda_D = (\varepsilon_0\varepsilon_f RT/2z^2F^2C_0)^{1/2}$ is the Debye length.

Solving eq 16 subject to eqs 7a and 8a, one gets

$$\psi = \frac{2RT}{zF}\ln\left[\frac{1+\exp(-\kappa x)\tanh(zF\psi_d/4RT)}{1-\exp(-\kappa x)\tanh(zF\psi_d/4RT)}\right] \tag{17}$$

and, therefore, the charge density of the diffusive layer is

$$\sigma_d = \frac{2\varepsilon_0\varepsilon_f\kappa RT}{zF}\sinh\left(\frac{zF\psi_d}{2RT}\right) \tag{18}$$

By integrating eq 4 twice with the boundary conditions described by eqs 7c and 8b, one obtains the pressure-driven flow velocity,

$$u_y = \frac{1}{2\mu}\frac{dp}{dy}(x^2 - hx) \tag{19}$$

where $-dp/dy = -\Delta p/l$ is the applied pressure gradient across the nanochannel.

Substituting eqs 15, 17, and 18 into eqs 11 and 12, we have the following implicit expressions relating the surface potential (ψ_s) to the zeta potential (ψ_d) of the nanochannel:

$$\begin{aligned} &-\varepsilon_0\varepsilon_d\left(\frac{\psi_s - V_g}{\delta}\right) + C_s(\psi_d - \psi_s) \\ &= FN_{total}\left\{\left[10^{-pK_A} - 10^{-pK_B}\left[10^{-pH}\exp\left(-\frac{F\psi_s}{RT}\right)\right]^2\right] \right. \\ &\left. \Big/\left[10^{-pK_A} + 10^{-pH}\exp\left(-\frac{F\psi_s}{RT}\right) + 10^{-pK_B}\left[10^{-pH}\exp\left(-\frac{F\psi_s}{RT}\right)\right]^2\right]\right\} \end{aligned} \tag{20}$$

and

$$-C_s(\psi_d - \psi_s) = \frac{2\varepsilon_0\varepsilon_f\kappa RT}{zF}\sinh\left(\frac{zF\psi_d}{2RT}\right) \tag{21}$$

For given conditions, one can easily use the Matlab function *fsolve* to determine both ψ_s and ψ_d by simultaneously solving eqs 20 and 21. Then, the electric potential (ψ) and the surface charge density of the diffusive layer (σ_d) can be probed by eqs 17 and 18, respectively, based on the resulting ψ_d.

The streaming current (I_{str}) through the nanochannel can be exactly evaluated by (see the detailed derivation in the Supporting Information)

$$\begin{aligned} I_{str} &= 2w\int_{\delta_s\to 0}^{h/2}\rho_e(x)u_y(x)dx \\ &= \frac{w\varepsilon_0\varepsilon_f h\psi_d\Delta p}{\mu l} - \frac{4w\varepsilon_0\varepsilon_f RT\Delta p}{\mu zF\kappa l} \\ &\left\{\left[\ln\left(\frac{1+A\exp(-\kappa h/2)}{1-A\exp(-\kappa h/2)}\right)\ln\left(\frac{2}{1-A\exp(-\kappa h/2)}\right) + \operatorname{dilog}\left(\frac{2}{1-A\exp(-\kappa h/2)}\right) + \operatorname{dilog}\left(\frac{1+A\exp(-\kappa h/2)}{1-A\exp(-\kappa h/2)}\right)\right] \right. \\ &\left. -\left[\ln\left(\frac{1+A}{1-A}\right)\ln\left(\frac{2}{1-A}\right) + \operatorname{dilog}\left(\frac{1+A}{1-A}\right) + \operatorname{dilog}\left(\frac{2}{1-A}\right)\right]\right\} \end{aligned} \tag{22}$$

where $A = \tanh(zF\psi_d/4RT)$ and dilog() represents the dilogarithm function. Once I_{str} is obtained, the streaming conductance (G_{str}) of the nanochannel can be determined by[42]

$$\begin{aligned} G_{str} &= I_{str}/(-\Delta p) \\ &= -\frac{w\varepsilon_0\varepsilon_f h\psi_d}{\mu l} + \frac{4w\varepsilon_0\varepsilon_f RT}{\mu zF\kappa l} \\ &\left\{\left[\ln\left(\frac{1+A\exp(-\kappa h/2)}{1-A\exp(-\kappa h/2)}\right)\ln\left(\frac{2}{1-A\exp(-\kappa h/2)}\right) + \operatorname{dilog}\left(\frac{2}{1-A\exp(-\kappa h/2)}\right) + \operatorname{dilog}\left(\frac{1+A\exp(-\kappa h/2)}{1-A\exp(-\kappa h/2)}\right)\right] \right. \\ &\left. -\left[\ln\left(\frac{1+A}{1-A}\right)\ln\left(\frac{2}{1-A}\right) + \operatorname{dilog}\left(\frac{1+A}{1-A}\right) + \operatorname{dilog}\left(\frac{2}{1-A}\right)\right]\right\} \end{aligned} \tag{23}$$

According to eqs 20–23, ψ_d, I_{str}, and, accordingly, G_{str} are functions of the gate potential (V_g), the surface capacitance of the Stern layer (C_s), the physicochemical properties of the dielectric channel wall (i.e., N_{total}, pK_A, pK_B, ε_d, and δ), and the solution properties (i.e., pH, C_{KCl}, and ε_f). It is worth noting that the present analytical MIM for the surface charge property and the streaming current/conductance in a gated nanochannel with and without FET control is more realistic and rigorous than most of the previous ones[6−8,28−40,42−48] due to the consideration of multiple ionic species, the Stern layer effect, and the surface chemistry reactions of the dielectric channel wall. The influence of H^+ and OH^- ions becomes significant when the solution pH is sufficiently high and low.

2.3. Analytical MIM Solution under the Debye–Hückel Approximation. Under the Debye–Hückel approximation (i.e., $|\psi_s| \ll RT/zF$), eqs 15 and 16 can be further approximated, respectively, to[40]

$$\sigma_s = -FN_{total}\left[\frac{\Phi}{\Omega} + \left(\frac{F\psi_s}{RT}\right)\left(\frac{\Pi}{\Omega} + \Lambda\right)\right] \tag{24}$$

and

$$\frac{d^2\psi}{dx^2} = \kappa^2\psi \quad \text{within the liquid phase} \quad (\delta_s \le x \le h/2) \tag{25}$$

In the above, $\Omega = 10^{-pK_A} + 10^{-pH} + 10^{-pK_B-2pH}$, $\Phi = 10^{-pK_A} + 10^{-pK_B-2pH}$, $\Pi = 2 \times 10^{-pK_B-2pH}$, and $\Lambda = \Phi(10^{-pH} + \Pi)/\Omega^2$.

Solving eq 25 subject to eqs 7a and 8a gives

$$\psi = \frac{\psi_d}{\sinh(\kappa h/2)} \sinh\left[\kappa\left(\frac{h}{2} - x\right)\right] \tag{26}$$

Therefore, the charge density of the diffusive layer σ_d can be described by

$$\sigma_d = \frac{\varepsilon_0\varepsilon_f\kappa\psi_d}{\tanh(\kappa h/2)} \tag{27}$$

By substituting eqs 24 and 27 into eqs 11 and 12, we obtain

$$-\varepsilon_0\varepsilon_d\left(\frac{\psi_s - V_g}{\delta}\right) - \frac{\varepsilon_0\varepsilon_f\kappa\psi_d}{\tanh(\kappa h/2)} = FN_{total}\left\{\frac{\Phi}{\Omega} + \left(\frac{F\psi_s}{RT}\right)\left(\frac{\Pi}{\Omega} + \Lambda\right)\right\} \tag{28}$$

and

$$-C_s(\psi_d - \psi_s) = \frac{\varepsilon_0\varepsilon_f\kappa\psi_d}{\tanh(\kappa h/2)} \tag{29}$$

Solving eqs 28 and 29 yields

$$\psi_s = \left\{\varepsilon_0\varepsilon_d V_g - \delta FN_{total}\left(\frac{\Phi}{\Omega}\right)\right\} \Big/ \left\{\varepsilon_0\varepsilon_d + \left[\left(\delta\varepsilon_0\varepsilon_f\kappa C_s\right)\Big/\left(C_s \tanh\left(\frac{\kappa h}{2}\right) + \varepsilon_0\varepsilon_f\kappa\right)\right] + \left[\frac{\delta F^2 N_{total}}{RT}\right]\left(\frac{\Pi}{\Omega} + \Lambda\right)\right\} \tag{30}$$

and

$$\psi_d = \left\{C_s\Big/\left[C_s + \left(\varepsilon_0\varepsilon_f\kappa/\tanh\left(\frac{\kappa h}{2}\right)\right)\right] \times \left[\left[\varepsilon_0\varepsilon_d V_g - \delta FN_{total}\left(\frac{\Phi}{\Omega}\right)\right] \Big/ \left[\varepsilon_0\varepsilon_d + \left[\delta\varepsilon_0\varepsilon_f\kappa C_s\Big/\left[C_s \tanh\left(\frac{\kappa h}{2}\right) + \varepsilon_0\varepsilon_f\kappa\right]\right] + \left(\frac{\delta F^2 N_{total}}{RT}\right)\left(\frac{\Pi}{\Omega} + \Lambda\right)\right]\right]\right\} \tag{31}$$

I_{str} and G_{str} can be further approximated, respectively, by (see the detailed derivation in the Supporting Information)

$$I_{str} = \frac{w\varepsilon_0\varepsilon_f\psi_d\Delta p}{\mu l}\left\{h + \frac{2[1 - \cosh(\kappa h/2)]}{\kappa \sinh(\kappa h/2)}\right\} \tag{32}$$

and

$$G_{str} = -\frac{w\varepsilon_0\varepsilon_f\psi_d}{\mu l}\left\{h + \frac{2[1 - \cosh(\kappa h/2)]}{\kappa \sinh(\kappa h/2)}\right\} \tag{33}$$

3. RESULTS AND DISCUSSION

To validate the derived models, section 3.1 compares the predictions of the streaming conductance, G_{str}, in a silica nanochannel from the analytical MIM to the existing experimental data available in the literature. The analytical MIM with the fitted parameters (i.e., N_{total}, pK_A, pK_B, and C_s) are then used to verify the applicability of that under the Debye–Hückel approximation in section 3.2, and to investigate the field effect regulation of the zeta potential and the streaming conductance in a gated silica nanochannel under various solution properties (pH and salt concentration) in sections 3.3 and 3.4. The relevant physical parameters used in the calculations are $\varepsilon_0 = 8.85 \times 10^{-12}$ C V^{-1} m^{-1}, $\mu = 10^{-3}$ kg m^{-1} s^{-1}, $F = 96487$ C mol^{-1}, $R = 8.31$ J K^{-1} mol^{-1}, $T = 298$ K, $\varepsilon_f = 78.5$, and $\varepsilon_d = 3.9$ (SiO_2).[29]

3.1. Verification of the Analytical MIM by Experimental Data.

The applicability of the present analytical MIM (eqs 20–23 in section 2.2) is first verified by the experimental data of van der Heyden et al.,[42] where the streaming conductance, G_{str}, in a silica nanochannel of width $w = 50$ μm and length $l = 4.5$ mm was conducted at the applied pressure $\Delta p = -4$ bar and pH = 8. Figure 2 depicts the dependence of G_{str} on the background salt concentration C_{KCl} for various nanochannel heights ranging from 140 to 1147 nm. As shown in Figure 2, the predictions from our analytical MIM (lines), with the same parameters $C_s = 0.42$ F/m^2, $N_{total} = 4$ nm^{-2}, $pK_A = 8$, and $pK_B = 2.5$, agree well with the experimental data of van der Heyden et al.[42] (symbols). The fitted parameters (i.e., C_s, N_{total}, pK_A, and pK_B) and the corresponding isoelectric point of the silica nanochannel (e.g., 2.75) are also consistent with those reported in the literature (e.g., N_{total} = 3.8–8 nm^{-2}, pK_A = 6–8, pK_B = 0–3, and C_s = 0.15–2.9 F/m^2 [7,42,45] and the isoelectric point is about 2–3.5[57] for the dielectric channel made of silica). It should be pointed out that only one set of the fitted parameters based on our model is used to describe the experimental data of the streaming conductance in a silica nanochannel with various channel heights. This is much better than the model proposed by van der Heyden et al.,[42] where they used different fitted parameters to describe the behaviors of the streaming conductance in the silica nanochannels with various heights. This might be caused by the neglection of multiple ionic species and the association

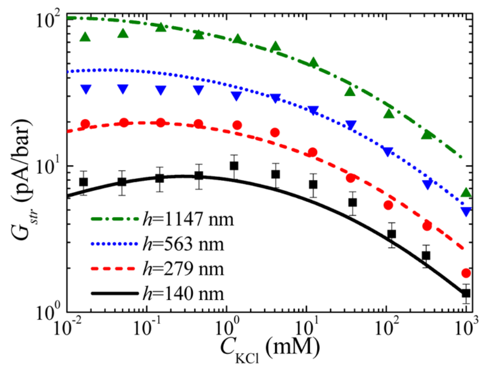

Figure 2. Dependence of the streaming conductance (G_{str}) in a silica nanochannel on the background salt concentration C_{KCl} for various nanochannel heights. Symbols: experimental data of van der Heyden et al.[42] at $\Delta p = -4$ bar, $w = 50$ μm, $l = 4.5$ mm, and pH = 8; lines: results of the present analytical MIM at $C_s = 0.42$ F/m^2, $N_{total} = 4$ nm^{-2}, $pK_A = 8$, and $pK_B = 2.5$.

dx.doi.org/10.1021/jp500996b | J. Phys. Chem. C 2014, 118, 6090–6099

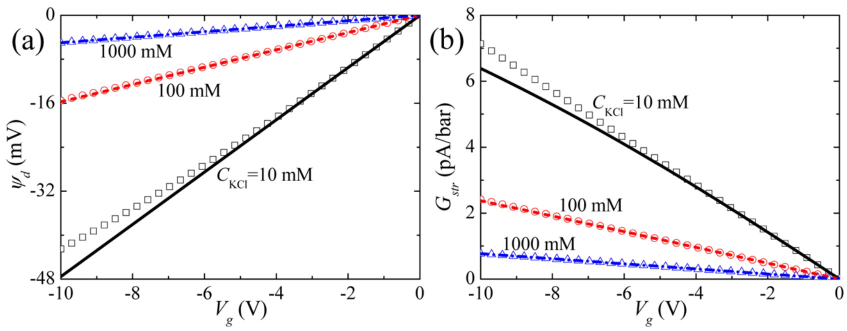

Figure 3. Zeta potential ψ_d (a) and streaming conductance G_{str} (b) as a function of the gate potential V_g for various background salt concentrations C_{KCl} at pH = 3. Symbols denote the results of the analytical MIM, and lines in (a) and (b) denote the results from the closed-form Debye−Hückel approximation based on eqs 31 and 33, respectively.

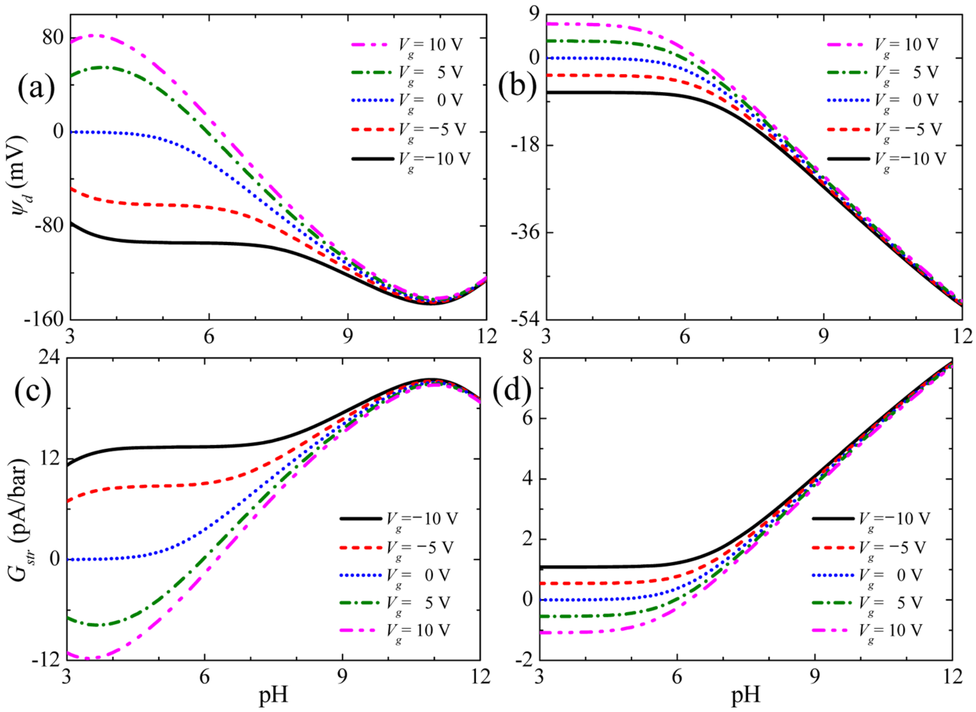

Figure 4. Zeta potential ψ_d (a, b) and streaming conductance G_{str} (c, d) as a function of the solution pH for various gate potential V_g at the background salt concentration C_{KCl} = 1 mM (a, c) and 500 mM (b, d).

reaction of silanol (Si−OH) groups on the nanochannel wall in their study. Therefore, the predicted values of $C_s = 0.42$ F/m^2, $N_{total} = 4$ nm^{-2}, pK_A = 8, and pK_B = 2.5, are then used in the following discussions. For illustration, we consider a FET-gated nanochannel with height h = 200 nm, width w = 50 μm, length l = 4.5 mm, and the thickness of the dielectric layer δ = 30 nm.

3.2. Verification of the Analytical MIM Solution under the Debye−Hückel Approximation. The applicability of the analytical MIM solutions under the Debye−Hückel approximation (i.e., $|\psi| \ll 25.7$ mV) for the zeta potential, ψ_d (eq 31), and the streaming conductance, G_{str} (eq 33), in a gated silica nanochannel is examined in Figure 3. In this figure, the variations of ψ_d and G_{str} as a function of the applied gate potential V_g for various background salt concentrations C_{KCl} at pH = 3 are plotted in Figure 3a and b, respectively. Figure 3 clearly shows that the results of ψ_d and G_{str} obtained from the closed-form analytical MIM solutions (eqs 31 and 33 in section 2.3) match well with those from the implicit solution based on the analytical MIM (eqs 20−23 in section 2.2). An excellent agreement between the results of ψ_d and G_{str} obtained from the above two models is observed when $|\psi_d|$ is below 25.7 mV at small V_g and high C_{KCl}. Even if $|\psi_d|$ is between 25.7 and 47.6 mV at large V_g and low C_{KCl}, a maximum relative error of about 10.6% between the closed-form analytical MIM expressions and the exact implicit solution obtained from the analytical MIM for ψ_d and G_{str} is obtained, as depicted in Figure 3. Therefore, we conclude that the present closed-form analytical MIM solutions are capable of accurately predicting the general trends of ψ_d and G_{str} for $|\psi_d| \leq 47.6$ mV, especially when the salt concentration is sufficiently high, which is the typical condition encountered in FET-gated nanofluidics applications.[20,25−27] Figure 3b also suggests that G_{str} is larger for lower C_{KCl}. This agrees with the experimental observations for the streaming current (or conductance),[6,7,42] and is because both the EDL thickness and the zeta potential (Figure 3a) of the nanochannel increase with a decrease in the salt concentration. These two combined effects lead to more net charges $(2w\int_{\delta_s}^{h/2}\rho_e(x)\mathrm{d}x)$ within the nanochannel carried by the pressure-driven flow. However, the salt concentration dependence of the streaming current/

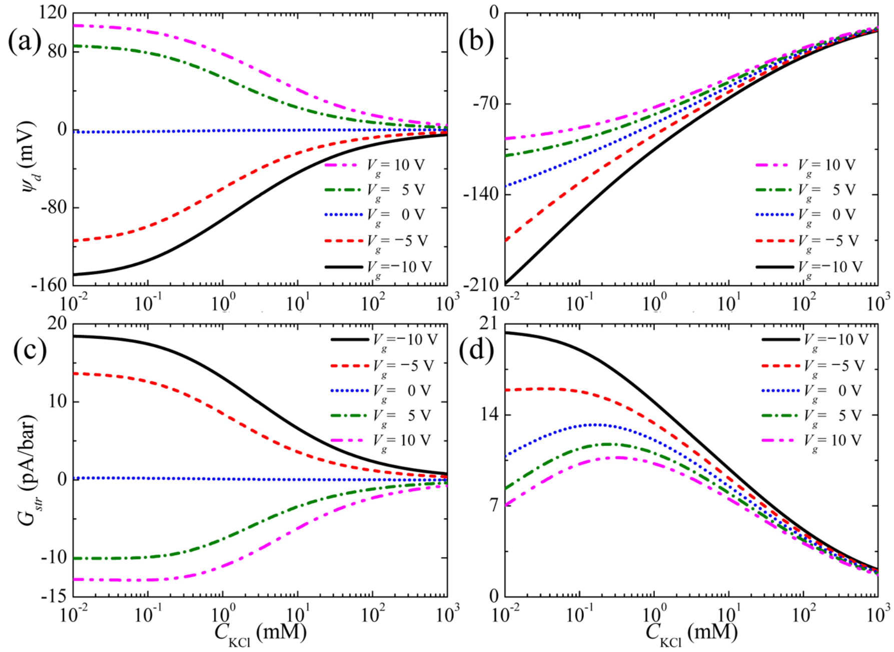

Figure 5. Zeta potential ψ_d (a, b) and streaming conductance G_{str} (c, d) as a function of the background salt concentration C_{KCl} for various gate potential V_g at the solution pH = 4 (a, c) and 8 (b, d).

conductance in the nanochannel is inconsistent with that of the ionic current/conductance, which decreases with a decrease in the salt concentration.[25] This is because the ionic current/conductance in nanofluidics is dominated by the net ionic concentration, $\sum_{i=1}^{N} C_{i0}$, in the bulk electrolyte solution[58] (not mobile net charges, ρ_e).

3.3. Influence of Solution pH. Figure 4 depicts the influence of the solution pH on the field effect regulation of the zeta potential, ψ_d, and the streaming conductance, G_{str}, for various gate potentials, V_g, at two levels of the background salt concentration, C_{KCl}. This figure clearly shows that the zeta potential, ψ_d, and, accordingly, the streaming conductance, G_{str}, of the nanochannel can be actively tuned from negative to positive by the gate potential, V_g. Similar behavior has been observed experimentally in the studies of the field effect control of the zeta potential in nanofluidics[20,41] and can be further utilized to control the transport of ions, fluid, and biomolecules.[20,25−27,35,41] Figure 4 also reveals that the performance of the field effect modulation of ψ_d (Figure 4a,b) and G_{str} (Figure 4c,d) is remarkable at low solution pH and becomes unremarkable at sufficiently high solution pH. This is because the proton concentration increases with decreasing solution pH, leading to less negatively charged SiO^- dissociated from the silanol (SiOH) functional groups on the nanochannel surface and, therefore, a smaller σ_s and lesser counterions electrostatically attracted to the channel surface, therefore, makes the FET easiler to tune its zeta potential. According to eqs 22 and 23, since the streaming current/conductance of the nanochannel strongly depends upon the magnitude of its zeta potential, a superior tuning efficiency of the streaming current by the FET in nanofluidics at low solution pH is observed in Figure 4c,d.

It is interesting to note in Figure 4 that the field effect regulation behaviors of ψ_d and G_{str} versus the solution pH depend significantly upon the levels of the applied gate potential V_g and the background salt concentration C_{KCl}. If the FET is floating (V_g = 0 V) and a negative gate potential is applied (V_g < 0 V), Figure 4b,d reveals that the magnitude of ψ_d and, accordingly, G_{str} increase monotonically with the solution pH at high salt concentration C_{KCl} = 500 mM. On the other hand, at relatively low salt concentration C_{KCl} = 1 mM (Figure 4a,c), both $|\psi_d|$ and G_{str} increase with the solution pH when it is low and show a local maximum when the solution pH is sufficiently high. The behavior that $|\psi_d|$ and, accordingly, G_{str}, increase with increasing pH is expected due to an increase in $|\sigma_s|$. However, an increase in the solution pH, when it deviates appreciably from 7, also results in an increase in the ionic strength (a decrease in the EDL thickness). If the behavior of ψ_d is dominated by the effect of an increase in the ionic strength, which becomes significant when C_{KCl} is sufficiently low, $|\psi_d|$ decreases accordingly. This explains why $|\psi_d|$ and, accordingly, G_{str} decrease with an increase in the solution pH for pH > 11 at C_{KCl} = 1 mM, as shown in Figure 4a,c.

If a positive gate potential is applied (i.e., V_g > 0 V), Figure 4a,b shows that ψ_d (G_{str}) remains negative (positive) at high solution pH and becomes positive (negative) at low solution pH. Note that when the solution pH is low, both ψ_d and $|G_{str}|$ show an apparent local maximum as the solution pH varies at low salt concentration C_{KCl} = 1 mM (Figure 4a,c) but decrease monotonically with increasing pH at high salt concentration C_{KCl} = 500 mM (Figure 4b,d). The former can be attributed to an increase in the ionic strength when the solution pH declines significantly from 7, thus, lowering the modulated zeta potential of the nanochannel. This effect becomes significant when the background salt concentration is sufficiently low, as described previously. From Figure 4, it is worth concluding that for a fixed C_{KCl}, the behavior of G_{str} as the solution pH varies is consistent with that of ψ_d because of the significant zeta potential-dependent streaming current (or conductance) behavior in the nanochannel, according to eqs 22 and 23.

3.4. Influence of Background Salt Concentration. Figure 5 depicts the influence of the background salt concentration, C_{KCl}, on the field effect regulation of the zeta potential, ψ_d, and the streaming conductance, G_{str}, for various gate potentials, V_g, at two levels of the solution pH. This figure shows that at low solution pH = 4, ψ_d and, accordingly, G_{str}, is modulated from negative to positive as V_g varies; however, only the magnitude of ψ_d and G_{str} can be tuned for the considered region of V_g ranging from −10 to 10 V at relatively high solution pH = 8. These behaviors are consistent with those in Figure 4 and can be attributed to a higher surface charge density of the nanochannel, thus making the FET harder to regulate the zeta potential and the corresponding electrokinetic transport phenomena in the nanochannel. Figure 5 also suggests that the degree of the field effect regulation of ψ_d (Figure 5a,b) and G_{str} (Figure 5c,d) is significant if C_{KCl} is low and becomes insignificant if C_{KCl} is sufficiently high. In this case, a higher gate potential is required to effectively tune the zeta potential and streaming current in the nanochannel.

Figure 5a,b reveals that regardless of the levels of pH and V_g, the magnitude of ψ_d decreases monotonically with increasing C_{KCl}. This is because the EDL thickness decreases with an increase in the salt concentration, resulting in more counterions gathered near the nanochannel wall and, thus, lowering its effective charge. It is interesting to note in Figure 5c,d that for the considered region of C_{KCl}, the behaviors of G_{str} with C_{KCl} depend upon the levels of pH and V_g. If the solution pH is low (Figure 5c), the magnitude of G_{str} increases with decreasing C_{KCl} in the high salt concentration regime and reaches a nearly saturated value (plateau) in the low salt concentration regime. On the other hand, if the solution pH is high (Figure 5d), G_{str} increases first and then attains a plateau as C_{KCl} decreases for the relatively high negative gate potentials (i.e., V_g = −5 and −10 V) and shows a local maximum for the floating FET (i.e., V_g = 0 V) and the positive gate potentials (i.e., V_g = 5 and 10 V). The local maximum of G_{str} extends to higher C_{KCl} for larger positive V_g. The behavior that G_{str} increases with a decrease in C_{KCl} in the high salt concentration regime can be attributed to the combined effects of a greater $|\psi_d|$ (shown in Figure 5a,b) and a thicker EDL. However, if C_{KCl} further declines to a critically low regime, because the major counterions (K^+ ions) from the background salt KCl become very dilute, G_{str} shows a decreasing tendency with a decrease in C_{KCl}. Note that if the solution pH is sufficiently low, the other counterions (H^+ ions) dissociated from HCl and water becomes dominant. Therefore, the aforementioned dilute effect of K^+ ions as C_{KCl} decreases becomes relatively insignificant. This is why G_{str} shows a plateau for lower C_{KCl} at the low solution pH, as seen in Figure 5c.

4. CONCLUSIONS

For the first time, we investigate the field effect control of the surface charge property and the streaming current/conductance, generated by a pressure-driven flow, in a FET-gated silica nanochannel under various solution properties (background pH and salt concentration). Taking practical effects such as multiple ionic species, surface chemistry reactions, and the Stern layer into account, we derived analytical expressions, including implicit and explicit ones, to estimate the surface charge property and the streaming current/conductance tuned by a FET. The implicit analytical multi-ion model (MIM) is validated by comparing its predictions to the existing experimental data of the streaming conductance in the silica nanochannels with various channel heights. The explicit analytical MIM based on the Debye−Hückel approximation is valid especially when the magnitude of the zeta potential is less than the thermal potential, which often holds for relatively high salt concentration, in accordance with typical nanofluidics-based experimental conditions. The results clearly show that the zeta potential as well as the streaming current/conductance can be actively tuned by the FET. The performance of the zeta potential and streaming conductance modulation by FET is better when the background salt concentration and pH are low. The developed model predicts that the dependence of the streaming conductance on the solution pH is consistent with the dependence of the zeta potential. However, that dependence on the salt concentration might be different from the dependence of the zeta potential, depending on the levels of the solution pH and the gate potential. For example, for relatively high solution pH, the magnitude of the zeta potential of the nanochannel increases with decreasing background salt concentration, but the streaming conductance increases first and then decreases (or exhibits a plateau) with a decrease in the salt concentration.

■ ASSOCIATED CONTENT

Supporting Information

The detailed derivation of eqs 22, 23, 32, and 33. This material is available free of charge via the Internet at http://pubs.acs.org.

■ AUTHOR INFORMATION

Corresponding Authors

*Fax: +886-5-5312071. E-mail: lhyeh@yuntech.edu.tw.
*E-mail: sqian@odu.edu.

Author Contributions

†These authors contributed equally to this work (S.X. and L.-H.Y.).

Notes

The authors declare no competing financial interest.

■ ACKNOWLEDGMENTS

This work is financially supported by the National Science Council of the Republic of China under Grants NSC-102-2221-E-224-052-MY3 and NSC-103-2218-E-002-010 (L.H.Y.), Innovative Research Groups of National Science Foundation of China under Grant No. 51121004 (Y.M.), and NSF DUE-0940895 (S.Q.).

■ REFERENCES

(1) Jiang, Y. N.; Liu, N. N.; Guo, W.; Xia, F.; Jiang, L. Highly-Efficient Gating of Solid-State Nanochannels by DNA Supersandwich Structure Containing ATP Aptamers: A Nanofluidic Implication Logic Device. *J. Am. Chem. Soc.* **2012**, *134*, 15395−15401.

(2) Zhang, H. C.; Hou, X.; Zeng, L.; Yang, F.; Li, L.; Yan, D. D.; Tian, Y.; Jiang, L. Bioinspired Artificial Single Ion Pump. *J. Am. Chem. Soc.* **2013**, *135*, 16102−16110.

(3) Karnik, R.; Duan, C. H.; Castelino, K.; Daiguji, H.; Majumdar, A. Rectification of Ionic Current in a Nanofluidic Diode. *Nano Lett.* **2007**, *7*, 547−551.

(4) Yameen, B.; Ali, M.; Neumann, R.; Ensinger, W.; Knoll, W.; Azzaroni, O. Single Conical Nanopores Displaying pH-Tunable Rectifying Characteristics. Manipulating Ionic Transport With Zwitterionic Polymer Brushes. *J. Am. Chem. Soc.* **2009**, *131*, 2070−2071.

(5) Vilozny, B.; Wollenberg, A. L.; Actis, P.; Hwang, D.; Singaram, B.; Pourmand, N. Carbohydrate-Actuated Nanofluidic Diode: Switchable Current Rectification in a Nanopipette. *Nanoscale* **2013**, *5*, 9214−9221.

(6) van der Heyden, F. H. J.; Bonthuis, D. J.; Stein, D.; Meyer, C.; Dekker, C. Electrokinetic Energy Conversion Efficiency in Nanofluidic Channels. *Nano Lett.* **2006**, *6*, 2232−2237.

(7) van der Heyden, F. H. J.; Bonthuis, D. J.; Stein, D.; Meyer, C.; Dekker, C. Power Generation by Pressure-Driven Transport of Ions in Nanofluidic Channels. *Nano Lett.* **2007**, *7*, 1022−1025.
(8) Yan, Y.; Sheng, Q.; Wang, C. M.; Xue, J. M.; Chang, H. C. Energy Conversion Efficiency of Nanofluidic Batteries: Hydrodynamic Slip and Access Resistance. *J. Phys. Chem. C* **2013**, *117*, 8050−8061.
(9) Siria, A.; Poncharal, P.; Biance, A. L.; Fulcrand, R.; Blase, X.; Purcell, S. T.; Bocquet, L. Giant Osmotic Energy Conversion Measured in a Single Transmembrane Boron Nitride Nanotube. *Nature* **2013**, *494*, 455−458.
(10) Bentien, A.; Okada, T.; Kjelstrup, S. Evaluation of Nanoporous Polymer Membranes for Electrokinetic Energy Conversion in Power Applications. *J. Phys. Chem. C* **2013**, *117*, 1582−1588.
(11) Howorka, S.; Siwy, Z. Nanopore Analytics: Sensing of Single Molecules. *Chem. Soc. Rev.* **2009**, *38*, 2360−2384.
(12) Vogel, R.; Anderson, W.; Eldridge, J.; Glossop, B.; Willmott, G. A Variable Pressure Method for Characterizing Nanoparticle Surface Charge Using Pore Sensors. *Anal. Chem.* **2012**, *84*, 3125−3131.
(13) Li, W.; Bell, N. A. W.; Hernandez-Ainsa, S.; Thacker, V. V.; Thackray, A. M.; Bujdoso, R.; Keyser, U. F. Single Protein Molecule Detection by Glass Nanopores. *ACS Nano* **2013**, *7*, 4129−4134.
(14) Schoch, R. B.; Han, J. Y.; Renaud, P. Transport Phenomena in Nanofluidics. *Rev. Mod. Phys.* **2008**, *80*, 839−883.
(15) Yeh, L. H.; Zhang, M.; Qian, S.; Hsu, J. P. Regulating DNA Translocation through Functionalized Soft Nanopores. *Nanoscale* **2012**, *4*, 2685−2693.
(16) Guo, W.; Tian, Y.; Jiang, L. Asymmetric Ion Transport through Ion-Channel-Mimetic Solid-State Nanopores. *Acc. Chem. Res.* **2013**, *46*, 2834−2846.
(17) Stein, D.; Kruithof, M.; Dekker, C. Surface-Charge-Governed Ion Transport in Nanofluidic Channels. *Phys. Rev. Lett.* **2004**, *93*, 035901.
(18) Siwy, Z. S. Ion-Current Rectification in Nanopores and Nanotubes with Broken Symmetry. *Adv. Funct. Mater.* **2006**, *16*, 735−746.
(19) Ali, M.; Ramirez, P.; Mafe, S.; Neumann, R.; Ensinger, W. A pH-Tunable Nanofluidic Diode with a Broad Range of Rectifying Properties. *ACS Nano* **2009**, *3*, 603−608.
(20) Karnik, R.; Fan, R.; Yue, M.; Li, D. Y.; Yang, P. D.; Majumdar, A. Electrostatic Control of Ions and Molecules in Nanofluidic Transistors. *Nano Lett.* **2005**, *5*, 943−948.
(21) Veenhuis, R. B. H.; van der Wouden, E. J.; van Nieuwkasteele, J. W.; van den Berg, A.; Eijkel, J. C. T. Field-Effect Based Attomole Titrations in Nanoconfinement. *Lab Chip* **2009**, *9*, 3472−3480.
(22) Hu, N.; Ai, Y.; Qian, S. Z. Field Effect Control of Electrokinetic Transport in Micro/Nanofluidics. *Sens. Actuators, B* **2012**, *161*, 1150−1167.
(23) Tsutsui, M.; He, Y.; Furuhashi, M.; Rahong, S.; Taniguchi, M.; Kawai, T. Transverse Electric Field Dragging of DNA in a Nanochannel. *Sci. Rep.* **2012**, *2*, 394.
(24) Paik, K. H.; Liu, Y.; Tabard-Cossa, V.; Waugh, M. J.; Huber, D. E.; Provine, J.; Howe, R. T.; Dutton, R. W.; Davis, R. W. Control of DNA Capture by Nanofluidic Transistors. *ACS Nano* **2012**, *6*, 6767−6775.
(25) Guan, W. H.; Fan, R.; Reed, M. A. Field-Effect Reconfigurable Nanofluidic Ionic Diodes. *Nat. Commun.* **2011**, *2*, 506.
(26) Guan, W. J.; Reed, M. A. Electric Field Modulation of the Membrane Potential in Solid-State Ion Channels. *Nano Lett.* **2012**, *12*, 6441−6447.
(27) Jiang, Z. J.; Stein, D. Charge Regulation in Nanopore Ionic Field-Effect Transistors. *Phys. Rev. E* **2011**, *83*, 031203.
(28) Daiguji, H.; Yang, P. D.; Majumdar, A. Ion Transport in Nanofluidic Channels. *Nano Lett.* **2004**, *4*, 137−142.
(29) Ai, Y.; Liu, J.; Zhang, B. K.; Qian, S. Field Effect Regulation of DNA Translocation through a Nanopore. *Anal. Chem.* **2010**, *82*, 8217−8225.
(30) Ai, Y.; Liu, J.; Zhang, B. K.; Qian, S. Ionic Current Rectification in a Conical Nanofluidic Field Effect Transistor. *Sens. Actuators, B* **2011**, *157*, 742−751.
(31) He, Y. H.; Tsutsui, M.; Fan, C.; Taniguchi, M.; Kawai, T. Gate Manipulation of DNA Capture into Nanopores. *ACS Nano* **2011**, *5*, 8391−8397.
(32) He, Y. H.; Tsutsui, M.; Fan, C.; Taniguchi, M.; Kawai, T. Controlling DNA Translocation through Gate Modulation of Nanopore Wall Surface Charges. *ACS Nano* **2011**, *5*, 5509−5518.
(33) Jin, X. Z.; Aluru, N. R. Gated Transport in Nanofluidic Devices. *Microfluid. Nanofluid.* **2011**, *11*, 297−306.
(34) Singh, K. P.; Kumar, M. Effect of Gate Length and Dielectric Thickness on Ion and Fluid Transport in a Fluidic Nanochannel. *Lab Chip* **2012**, *12*, 1332−1339.
(35) Matovic, J.; Adamovic, N.; Radovanovic, F.; Jaksic, Z.; Schmid, U. Field Effect Transistor Based on Ions as Charge Carriers. *Sens. Actuators, B* **2012**, *170*, 137−142.
(36) Xue, S.; Hu, N.; Qian, S. Z. Tuning Surface Charge Property by Floating Gate Field Effect Transistor. *J. Colloid Interface Sci.* **2012**, *365*, 326−328.
(37) Benson, L.; Yeh, L. H.; Chou, T. H.; Qian, S. Z. Field Effect Regulation of Donnan Potential and Electrokinetic Flow in a Functionalized Soft Nanochannel. *Soft Matter* **2013**, *9*, 9767−9773.
(38) Pardon, G.; van der Wijngaart, W. Modeling and Simulation of Electrostatically Gated Nanochannels. *Adv. Colloid Interface Sci.* **2013**, *199*, 78−94.
(39) Yeh, L. H.; Xue, S.; Joo, S. W.; Qian, S.; Hsu, J. P. Field Effect Control of Surface Charge Property and Electroosmotic Flow in Nanofluidics. *J. Phys. Chem. C* **2012**, *116*, 4209−4216.
(40) Hughes, C.; Yeh, L. H.; Qian, S. Field Effect Modulation of Surface Charge Property and Electroosmotic Flow in a Nanochannel: Stern Layer Effect. *J. Phys. Chem. C* **2013**, *117*, 9322−9331.
(41) Guan, W. H.; Rajan, N. K.; Duan, X. X.; Reed, M. A. Quantitative Probing of Surface Charges at Dielectric-Electrolyte Interfaces. *Lab Chip* **2013**, *13*, 1431−1436.
(42) van der Heyden, F. H. J.; Stein, D.; Dekker, C. Streaming Currents in a Single Nanofluidic Channel. *Phys. Rev. Lett.* **2005**, *95*, 116104.
(43) Daiguji, H.; Yang, P. D.; Szeri, A. J.; Majumdar, A. Electrochemomechanical Energy Conversion in Nanofluidic Channels. *Nano Lett.* **2004**, *4*, 2315−2321.
(44) Wang, M. R.; Kang, Q. J. Electrochemomechanical Energy Conversion Efficiency in Silica Nanochannels. *Microfluid. Nanofluid.* **2010**, *9*, 181−190.
(45) Andersen, M. B.; Bruus, H.; Bardhan, J. P.; Pennathur, S. Streaming Current and Wall Dissolution over 48 h in Silica Nanochannels. *J. Colloid Interface Sci.* **2011**, *360*, 262−271.
(46) Chang, C. C.; Yang, R. J. Electrokinetic Energy Conversion in Micrometer-Length Nanofluidic Channels. *Microfluid. Nanofluid.* **2010**, *9*, 225−241.
(47) Chang, C. C.; Yang, R. J. Electrokinetic Energy Conversion Efficiency in Ion-Selective Nanopores. *Appl. Phys. Lett.* **2011**, *99*, 083102.
(48) Das, S.; Guha, A.; Mitra, S. K. Exploring New Scaling Regimes for Streaming Potential and Electroviscous Effects in a Nanocapillary with Overlapping Electric Double Layers. *Anal. Chim. Acta* **2013**, *804*, 159−166.
(49) Behrens, S. H.; Grier, D. G. The Charge of Glass and Silica Surfaces. *J. Chem. Phys.* **2001**, *115*, 6716−6721.
(50) Jiang, Z. J.; Stein, D. Electrofluidic Gating of a Chemically Reactive Surface. *Langmuir* **2010**, *26*, 8161−8173.
(51) Stein, D.; Deurvorst, Z.; van der Heyden, F. H. J.; Koopmans, W. J. A.; Gabel, A.; Dekker, C. Electrokinetic Concentration of DNA Polymers in Nanofluidic Channels. *Nano Lett.* **2010**, *10*, 765−772.
(52) Louer, A. C.; Plecis, A.; Pallandre, A.; Galas, J. C.; Estevez-Torres, A.; Haghiri-Gosnet, A. M. Pressure-Assisted Selective Preconcentration in a Straight Nanochannel. *Anal. Chem.* **2013**, *85*, 7948−7956.
(53) Startsev, M. A.; Inglis, D. W.; Baker, M. S.; Goldys, E. M. Nanochannel pH Gradient Electrofocusing of Proteins. *Anal. Chem.* **2013**, *85*, 7133−7138.

(54) Yeh, L. H.; Zhang, M.; Qian, S.; Hsu, J. P.; Tseng, S. Ion Concentration Polarization in Polyelectrolyte-Modified Nanopores. *J. Phys. Chem. C* **2012**, *116*, 8672−8677.
(55) Yeh, L. H.; Zhang, M. K.; Joo, S. W.; Qian, S.; Hsu, J. P. Controlling pH-Regulated Bionanoparticles Translocation through Nanopores with Polyelectrolyte Brushes. *Anal. Chem.* **2012**, *84*, 9615−9622.
(56) Yeh, L. H.; Zhang, M.; Qian, S. Ion Transport in a pH-Regulated Nanopore. *Anal. Chem.* **2013**, *85*, 7527−7534.
(57) Kosmulski, M. pH-Dependent Surface Charging and Points of Zero Charge. IV. Update and New Approach. *J. Colloid Interface Sci.* **2009**, *337*, 439−448.
(58) Yeh, L. H.; Zhang, M.; Hu, N.; Joo, S. W.; Qian, S.; Hsu, J. P. Electrokinetic Ion and Fluid Transport in Nanopores Functionalized by Polyelectrolyte Brushes. *Nanoscale* **2012**, *4*, 5169−5177.